

DUOPLASMATRON SOURCE PERFORMANCE AT MURA

J. A. Fasolo, C. D. Curtis, and G. M. Lee
Midwestern Universities Research Association
Stoughton, Wisconsin

Abstract

A duoplasmatron with an expanded plasma front and a Pierce-electrode extraction geometry has been under development at MURA since September, 1965. Modifications of expansion cup, magnetic aperture, plasma-defining aperture, intermediate electrode, and extraction geometries to increase beam current and improve beam quality are reviewed. A source point correction to emittance estimates is derived. Emittance estimates, beam characteristic curves, and some results of mass analysis are presented and discussed. Results of a constant perveance experiment are given. A transition region in the beam characteristic curves is related to plasma boundary shape and beam quality. A magnetic field shaping experiment is discussed. Results of a bench test of the pre-accelerator extractor and focus electrode geometry are presented.

Introduction

On the basis of encouraging results obtained at Saclay¹ with a Pierce-electrode extraction geometry for a duoplasmatron with an expanded plasma front, an ion source with Pierce-type electrodes was designed and built in the summer of 1965 and put into operation in September of that year. The objective, which has still to be achieved, was to obtain a parallel beam of several hundred milliamperes of H^+ of quality suitable for injection into a high gradient preaccelerator column.

Source Assembly, Geometry 1

Geometry 1 is shown in Fig. 1. The extraction geometry was designed to accelerate, in the ideal case, a 9/16-in. diameter parallel beam across a 9/16-in. gap. The magnetic field was reduced to a negligible value in the extraction region by using a mild steel plasma-defining aperture and a relatively large drift

space between the aperture and the extraction region. It was thought that this was necessary to avoid the defocusing effect of a diverging magnetic field in a region of low particle energy. A defocusing effect was considered undesirable, as it would convert an initially uniform distribution of particles into a nonuniform distribution because of differences in the amounts of defocusing for the various components of the beam. Such a change in distribution could result in distortions that might be mistaken for lens aberrations in the preaccelerator column.

Target Assembly

The beam current obtained with Geometry 1 was measured with a target assembly consisting of a shield with a 2.000-in. diameter aperture, followed by a bias grid of parallel 0.010-in. diameter tungsten wires at intervals of 0.100 in., followed by a 0.005-in. thick copper target plate with 0.015-in. diameter apertures at 0.200-in. intervals along the x- and y- axes, followed by an aluminized fluorescent screen 2.000 in. from the target plate. The entire assembly can be moved in the z direction, or rotated about an axis 2-7/8 in. above the beam axis. The phosphor screen has since been replaced with aluminized quartz or Vycor plates. Slit images are photographed through a lucite light pipe used to attenuate the x-ray flux out through the viewing port.

The collimator in front of the bias grid is connected to ground through a 10-ohm metering resistor. The bias grid is connected to a 1000-volt supply of negative voltage, and the target plate and screen portion of the assembly is connected to ground through a 10-ohm metering resistor. The voltage developed across this resistor is displayed on a two-channel oscilloscope, along with the voltage from the low resistance side of a 10,000 to 1 compensated divider which measures extraction voltage.

There is little change in the indicated beam current after the bias voltage is raised above

Work performed under the auspices of the U. S. Atomic Energy Commission.

50 volts, and the grid is generally operated at 300 volts. Corrections for secondary electrons with energies greater than 300 volts and for secondary electrons originating at the grid and accelerated to the target plate are not known. A 10 per cent correction for beam intercepted by the bias grid is not normally added to the beam current read on the oscilloscope and has not been used for any of the currents given in this report.

The target plate with the circular apertures has since been replaced with a 0.005-in. thick copper slit plate with 0.015-in. wide slits at 0.200-in. intervals. The slits are bridged at 0.430-in. intervals for support.

Results Obtained with Geometry 1

The maximum current obtained with Geometry 1 for an extraction voltage of 60 kV and a pulsed arc current of about 27 amperes (six 200 μ sec pulses per second) was approximately 38 mA. The beam was highly divergent and gave multiple images of each of the circular holes in the target plate, which was located several inches from the extractor.

Cup Geometry and Magnetic Field Modifications

A number of changes followed, with the general trend being toward a larger magnetic aperture and a smaller expansion cup volume. The plasma-defining aperture was held constant at 0.052-in. diameter by using a nonmagnetic anode aperture plate. Geometry 6 gave in excess of 300 mA at 60 kV. The target plate with circular holes had been replaced with a slit plate, described above, and distorted multiple images were still prominently in evidence.

Modifications to Improve Beam Quality

Whereas the previous modifications were aimed at getting a larger beam current, a number of modifications were now made to improve beam quality.

Extraction Grid

A tungsten grid (2.4 mil wire, 77.4 per cent transparency) was spot welded to the beam exit side of the extractor. Geometry 9 gave a 55 mA, 16 keV beam with a radius $r_{\max} = 0.81$ in. and a divergence $\tan \theta_{\max} = 0.28$ on a slit plate 2-1/16 in. from the extractor. Secondary images of the slits were absent. When the

extraction voltage was increased to 44 kV, a smaller diameter highly distorted 180 mA beam was obtained. The extrapolated current for constant perveance should have been 245 mA. It was therefore concluded that a plasma sufficiently dense to give a 245 mA (and, hopefully, distortion free) beam could not be produced with this geometry and the limited arc current from the existing arc supply.

Modified Intermediate Electrode

Several changes in geometry that increased the magnetic aperture in the anode still further brought the maximum distortion-free beam up to approximately 75 mA.

In Geometry 14, the conventional intermediate electrode bore was abandoned in favor of a new design.² The new design (see Fig. 2) was based on several suppositions. First, that attenuation of the plasma occurs in the bore of the conventional intermediate electrode because of ion losses to the cylinder wall in the first portion of the bore, where the magnetic field is negligible. Second, that the resulting neutrals have a significantly high probability of emerging from the intermediate electrode into a region that is not occupied by plasma. Third, that the remaining lower density plasma is funneled down by the mirror effect of the rapidly increasing magnetic field to such a small diameter that an insufficient amount of gas diffuses into and becomes ionized by the arc to compensate for ion losses (elsewhere) and sustain the desired degree of ionization.³ During a short pulse, the rate at which gas is consumed may be less than, equal to, or greater than the rate at which it is supplied, during all or any part of the pulse.⁴

A flux plot, with Geometry 30 superimposed, is shown in Fig. 3. The plot, obtained with the aid of an electrolytic tank using a method suggested to us by E. M. Rowe, shows that in the new design the magnetic field penetrates further into the cathode-intermediate electrode region than in the conventional design. Ions recombining on the wall in this region are more apt than not to result in neutrals that are directed toward the cathode and these are less likely to emerge from the source without being reionized.

If there were no diffusion of ions across the magnetic field in the space between the intermediate electrode and the anode, the plasma would be confined within a flux tube that grazes the

edges of the intermediate electrode aperture, the anode aperture, and the Pierce electrode. This was one of the design objectives, to insure proper expansion of the plasma with a minimum of ion losses to the expansion cylinder wall. Erosion of the conical surface of the intermediate electrode bore indicates that the plasma does diffuse across the magnetic field to an appreciable extent, at least for the lower magnetic fields.

Distortion-free beams with currents of the order of 130 mA and energies of the order of 20 keV were obtained with Geometry 14, but the beam radius and divergence were so large they could not be measured with our target assembly.

Improved Extraction Grid Geometry

In Geometry 18, the grid on the beam exit side of the extractor was replaced with a grid stretched over the entire face of the electrode as shown in Fig. 2. Because of an anode modification that failed to work as anticipated, the full benefit of the new grid was not obtained in Geometry 18. This design feature was removed and, with Geometry 21, a distortion-free 190 mA, 25 keV beam with $r_{\max} = 0.875$ in. and $\tan \theta_{\max} = 0.285$ was obtained on a slit plate 2-1/16 in. from the extractor grid.

Changes in Extraction Geometry

Several minor modifications were made with no significant improvement over the results cited above for Geometry 21. This geometry, with the extractor grid removed, was then re-installed. The resulting geometry, Geometry 24, is shown in Fig. 4, together with data showing the variation of beam current and beam quality with increasing magnetic field. It may be noted that in every case the beam is highly distorted, with multiple images of each slit.

Stretching a flat grid across the expansion cup (somewhat to the left of the proper location) gave little, if any, improvement as may be seen in Fig. 4, Geometry 25.

Replacing the grid with a stainless steel ring (Geometry 26, Fig. 5) eliminated on-axis distortions and reduced off-axis distortions for the higher beam currents. Replacing the ring with a tapered stainless steel cylinder (Geometry 28, Fig. 5) reduced distortions still further, leaving only very weak secondary images of the slits farthest off-axis for the higher currents.

The extraction grid was reinstalled in Geometry 29 (Fig. 5). For beam currents of 120 mA or more the images are distortion free, but r_{\max} and $\tan \theta_{\max}$ are quite large.

Multiple Aperture Anode Inserts

The results obtained up to this point indicated we could get a distortion-free beam with good emittance, but only for highly divergent beams. It was thought that this might be due to a nonuniform density distribution in the plasma, with the highest density occurring on the axis. The density of plasma emerging from a single aperture is always highest on the axis of the aperture but with proper spacing of multiple apertures, the overall density distribution can be smoothed out, to some extent.

The anode insert with a single 0.052-in. diameter aperture on axis was replaced in Geometry 31 by an insert having a square array of nine 0.025-in. diameter holes at 0.0425-in. intervals. This geometry gave a slight decrease in divergence but the maximum current was down by a factor of 2. When the center aperture was blocked off, leaving a blank area 0.060 in. on a side, the beam current was reduced by another factor of 2.

The nine-hole aperture plate was then replaced with a 0.040-in. thick copper plate having three 0.032-in. diameter holes equally spaced on a 0.052-in. diameter circle. Some results obtained with this type of aperture are shown in Fig. 6 for Geometry 35. Smaller diameter, lower divergence, distortion-free beams are obtained with this aperture plate than with the previous single hole anode insert, but the currents for these beams are also smaller and the divergence is still quite large at higher perveance.

Emittance Estimates

Source Point Correction

Most of our estimates of emittance have been made for diverging distortion-free beams, with a source point correction^{5,6} to the measured divergence of the beam emerging from the on-axis slit. A derivation of the correction follows.

The emittance diagram for a zero-emittance laminar-flow beam diverging from a virtual source point is a straight line whose equation can be written as

$$\theta = \frac{r}{z_s} \quad (1)$$

where z_s is the distance from the measuring plane (slit plate) to the virtual source point from which the beam appears to be diverging. If we now permit this laminar-flow beam to have a finite emittance, the emittance diagram will be a symmetrical figure whose boundary equation can be written in the form

$$\theta = \frac{r}{z_s} \pm \alpha(r), \quad (2)$$

where $\alpha(r)$ is that part of the divergence due to finite emittance. In the most frequently employed method of plotting emittance, the values of θ that are plotted for $r = 0$ are given by

$$\theta(0) = \pm \left[\frac{W}{2z_s} + \alpha\left(\frac{W}{2}\right) \right], \quad (3)$$

where W is the slit width. The correct value is

$$\theta(0) = \pm \alpha(0), \quad (4)$$

which is not given by our measurements. If we assume $\alpha(0) \simeq \alpha\left(\frac{W}{2}\right)$, we can plot $\theta(0) = \pm \alpha\left(\frac{W}{2}\right)$ and make similar corrections for off-axis slits. If the emittance diagram is an ellipse, the correct area is given by

$$\pi ab \simeq \pi \alpha(0) r_{\max} \simeq \pi \alpha\left(\frac{W}{2}\right) r_{\max}, \quad (5)$$

and this can be written in the form

$$\pi \alpha\left(\frac{W}{2}\right) r_{\max} = \pi \left[\theta\left(\frac{W}{2}\right) - \frac{W}{2z_s} \right] r_{\max} \quad (6)$$

where $\theta\left(\frac{W}{2}\right)$ is the measured divergence at the edge of the on-axis slit and $\frac{W}{2z_s}$ is the source point correction. The normalized emittance is then given by

$$v = \beta \gamma \alpha\left(\frac{W}{2}\right) r_{\max}. \quad (7)$$

Photographic Measurements

The photographic method we have been using to study beam quality is quite useful in comparing different geometries or different operating conditions for the same geometry. It has its limitations, however, when we try to estimate emittance from measurements on the photographs. There is some uncertainty with regard to proper exposure and we have, therefore, tried to be conservative in choosing the exposure. A serious problem results from the fact

that the width of a slit image is usually of the order of 0.030 in. and this is reduced to about 0.010 in. (the ratio is 3.28 for our most recent work) on the photograph. Our measurements of photographic line width are good to about 1 mil for a sharply defined line. For our target geometry and the above ratio of 3.28, $\theta\left(\frac{W}{2}\right)$, in milliradians, is given by

$$\theta\left(\frac{W}{2}\right) = 0.82 W_m - 3.75 \quad (8)$$

where W_m is the measured photographic line width of the on-axis slit image, in mils. The source point correction, $W/2z_s$, is usually of the order of 2.5. For $W_m = 10$, $\theta\left(\frac{W}{2}\right) = 4.5$, and a 1 mil error in measuring line width will result in a large error in our estimate of emittance using Eqs. (6) or (7).

In most of our work, we have kept the exposure time constant for all of the photographs in a given sequence of data sets or varied it arbitrarily to compensate for obvious over or under exposures. It would, however, be preferable to vary the exposure according to the equation given by Spangenberg⁷ for exposure time in the photography of recurrent traces:

$$t = \frac{K F^2 (M+1)^2}{w} \quad (9)$$

where K is a constant chosen to give a suitable exposure, F is lens stop, M is image magnification and w is beam power density.

Use of this equation requires a suitable choice for the constant, a determination of beam power density for each set of data and one or more trial photographs to get the proper exposure for each set of data. Because of the great amount of time required to do this, and the possibility of fluctuations in source operating parameters while it is being done, this procedure has been carried out on a few occasions only.

Some Emittance Estimates

We have stated above that for Geometry 29 (Fig. 5) distortion-free images are obtained for beam currents of 120 mA or more. For each of the three data sets to which this applies we estimate a normalized emittance of 0.033 mrad-cm. The exposure time was kept constant and beam power density decreased with increasing beam current.

Emittance estimates and a quantity proportional to beam power density are shown in Fig. 6 for Geometry 35. Exposure time was kept constant. Beam power density goes through a minimum at 63 mA of beam current and then increases rapidly. The fluctuation in emittance for the lower beam currents is probably due to our inability to measure line widths accurately, coupled with a rapid change in $\alpha(\frac{W}{2})$ with line width. For beam currents greater than 63 mA there is a definite broadening of the lines due in part, at least, to our failure to adjust exposure time with varying beam power density.

A constant perveance experiment in which an attempt was made to vary exposure time according to Eq. (9) will be discussed in a later section.

Beam Characteristic Curves and Magnetic Analysis

For a sequence of data sets such as that shown in Fig. 6, in which magnet current is the variable, curves can be drawn giving the variation of beam radius and divergence with perveance. If several runs are made with different arc currents, families of characteristic curves are obtained (see Fig. 7). For each arc current, there is a transition region in which r_{max} and $\tan \theta_{max}$ are multiple-valued functions of perveance. Below the transition region, a distorted beam is obtained; above, the beam is distortion free. There is a significant increase in beam loading on the extraction voltage in the transition region and it is thought that the transition occurs when the beam diameter at the extractor becomes as large or slightly larger than the aperture in the extraction electrode.

As the arc current is increased, the characteristic curves are shifted in the direction of increasing perveance. For an ideal Pierce geometry with 100 per cent transmission, the beam current in the gap would be given by

$$I_{mA} = \frac{5.40 V_{kV}^{3/2}}{M^{1/2}(z_0/r_e)^2} = P_s V_{kV}^{3/2} \quad (10)$$

where

$$M^{1/2} = \frac{I_{H1}^+}{I_{mA}} + \sqrt{2} \frac{I_{H2}^+}{I_{mA}} + \sqrt{3} \frac{I_{H3}^+}{I_{mA}} \quad (11)$$

is the square root of the effective mass, r_e the constant beam edge radius and z_0 is the constant value of the distance from the plasma

boundary to the extractor. In the actual source, the source perveance P_s is a function of the three variables $M^{1/2}$, r_e , and z_0 and, since the plasma boundary is no longer plane, the constant in Eq. (10) is no longer correct.

Space-charge spread of the beam emerging from the source is given, in the ideal case, by

$$\frac{z}{r_0} = \frac{4.94}{M^{1/4}} \frac{V_{kV}^{3/4}}{I_{mA}^{1/2}} \int_1^R \frac{dR}{\sqrt{\ln R}} \quad (12)$$

where $R = r_e/r_0$ and r_0 is the value of r_e at the extractor. Substituting from (10),

$$\frac{z}{r_0} = \frac{4.94}{\sqrt{5.40}} \left(\frac{z_0}{r_0}\right) \int_1^R \frac{dR}{\sqrt{\ln R}} \quad (13)$$

For the actual source, with a nonplanar variable plasma boundary, the constant $4.94/\sqrt{5.40}$ would have to be replaced by a function of the variables z_0 and r_e , and the integral would have to be modified to account for initial beam divergence. The point we wish to make, however, is that for a given plasma boundary the perveance is a function of $M^{1/2}$ while the particle trajectories are independent of M . Thus we would expect that for given values of r_{max} and $\tan \theta_{max}$ the perveance and the effective mass would be related by the equation

$$P_s M^{1/2} = \text{const.} \quad (14)$$

The shift of the characteristic curves to higher perveance with increasing arc can thus be attributed to a corresponding decrease in $M^{1/2}$.

A mass analysis of the beam was made to verify this. The source was operated under conditions approximating those for the 0.630, 0.668, and 0.708 perveance points on the 24, 30, and 48 ampere arc curves for r_{max} and $\tan \theta_{max}$. The results are presented in Table I.

Table I

Results of Experiment on Constancy of $P_s M^{1/2}$

I_{arc}	I_{mag}	P_s	$M^{1/2}$	$P_s M^{1/2}$
24 A	0.51 A	0.630	1.28	0.812
30	0.50	0.668	1.14	0.762
48	0.36	0.708	1.12	0.793

The relative abundance of each beam component is given in Table II.

Table II

Results of Mass Analysis

I_{arc}	I_{mag}	H^+	H_2^+	H_3^+
24 A	0.51 A	62.8 %	30.4 %	6.8 %
30	0.50	68.4	27.8	3.8
48	0.36	71.7	26.1	2.2

The proton percentage increases with magnet current and results obtained at a higher magnet current are presented in Table III.

Table III

Results of Mass Analysis

I_{arc}	I_{mag}	H^+	H_2^+	H_3^+
24 A	0.71 A	77 %	21 %	2.0 %
30	0.71	80	20	0.0
48	0.71	86	14	0.0

All of the above results were obtained with a source pressure of approximately 200μ as measured with a thermocouple gauge calibrated for air. Lower pressures gave higher percentages of molecular ions and were, therefore, of less interest for our application.

A Constant Perveance Experiment

In this experiment, the source was adjusted to give a full image of the on-axis beam, with no bridge cutoff of the beam edge by the slit plate. Visual observation of the beam current and extraction voltage wave forms, subject to error because of parallax, yielded a calculated perveance of $0.750 \text{ mA}/(\text{kV})^{3/2}$. An exposure time of 60 seconds with $F = 8$ appeared to be suitable

for the first set of data and exposure time was varied according to Eq. (9) by keeping the product $tV^{5/2}$ constant for the remaining data sets as the extraction voltage was varied in two kilovolt steps and the source was adjusted to give the appropriate current for a perveance of $0.750 \text{ mA}/(\text{kV})^{3/2}$. It was assumed on the basis of previous experience that r_{max} would be constant and would not have to be considered in the calculation of exposure time. The camera shutter was actuated by an automatic timer.

At the completion of the experiment, measurements on photographs of the beam current and extraction voltage waveforms, with zero-signal traces superimposed, revealed that the perveance was somewhat higher than the value calculated from visual observation of the signals so that the exposure time variation was not quite correct.

The results of the experiment, shown in Fig. 8, were as expected, with two notable exceptions. It was not anticipated that the source point correction would be greater than the measured divergence at the edge of the on-axis slit, yet we find $\theta (\frac{W}{2}) = 2.0 \text{ mrad}$ and $\frac{W}{2z_s} = 2.3 \text{ mrad}$, using average values of r_{max} , $\tan \theta_{max}$, and W_m , the photographic line width. This result merely emphasizes what we have said above about our uncertainty as to the correct exposure and our inability to measure the line widths with sufficient accuracy. It also suggests that the emittance is quite small.

If we ignore the source point correction altogether, we find $\pi \theta (\frac{W}{2}) r_{max} = 11 \text{ mrad-cm}$ which is somewhat smaller than the lowest value obtained by H. Wroe⁸ when he used 10 mil slits (14 mrad-cm) but considerably larger than the value of 2.6 mrad-cm that he obtained with 2 mil diameter pin holes. Wroe, working with higher density beams than we have used, showed that there could be a significant amount of space-charge spreading of the individual beams emerging from the slit plate before they reached the target plate. By going to pin holes, he reduced the space-charge effect and the source point correction.

The other exception to our expectations is the linear variation in magnet current with extraction voltage. After we had verified the constancy of the beam radius and divergence, and concluded that the location and shape of the plasma boundary were essentially constant in this experiment, idle curiosity led us to check

the variation of magnetic field against the behavior expected from the well known scaling law^{9, 10}

$$\frac{V}{B^2 L^2} = \text{const.}$$

The fact that the scaling law is not satisfied suggests that the magnetic field in the extraction region is too weak to have a measurable affect on particle trajectories. However, in a later section we will describe an experiment in which the shape of the magnetic field, if not its magnitude, has an easily measurable affect on particle trajectories in the extraction region.

Although we have no absolute measure of the emittance, we may conclude from this experiment that when the perveance is kept constant the emittance varies as the one-third power of the beam current, or as $B^{1/2}$ over the range of magnet currents that we have covered.

It should be mentioned that we have no accurate method of measuring or controlling the thickness of the aluminum coating on our target plates. Occasionally this produces a plate that transmits light from the arc, resulting in the bright spot seen at the centers of the beam images shown in Fig. 8.

Plasma Boundary Shape and Beam Quality

The presence of a transition region in the beam characteristic curves and the marked difference in beam quality below and above the transition, coupled with a significant increase in beam loading on the extraction voltage in the transition region suggests that as the perveance increases the plasma boundary, which may be concave at very low perveance, advances toward the extractor and becomes increasingly convex. In the transition region the beam current and the perveance go through a local minimum and then increase again as beam loss to the extractor is offset by a reduction in accelerating gap and a consequent increase in the total space-charge limited current. Improvement in beam quality above the transition region may be attributed to the fact that diverging beam edge particles which, at lower perveance, encounter a sufficiently strong radial focusing field to squeeze them through the extractor aperture are scrapped off by the extractor at higher perveance. The diverging edge particles which are forced through the extractor aperture by the radial field at lower perveance will appear to

come from a different source point than particles inside the beam which are not influenced by the radial field outside the beam edge and this will result in multiple slit images that may or may not be completely resolved at the location of the target plate.

As the plasma boundary becomes more convex, the electric and magnetic fields in its immediate neighborhood become more nearly parallel at all distances from the axis. The reduced affect of crossed fields on low energy particles in this region, and particularly off axis, may also result in an improvement in beam quality.

Although there is no doubt that we do not have a Pierce geometry when we obtain our best quality beams, two experiments were performed to give us a better insight into the degree of departure from the ideal geometry. The first of these is shown in Fig. 9 for Geometry 36, where a stainless steel insert was used to destroy any semblance to a Pierce geometry. There are no resolved multiple images and the beam quality, while not good, is better than that for some of our earliest attempts to achieve a Pierce geometry. In the second experiment, shown in Fig. 10, the insert was tapered to give a better match in the field at the beam edge for a convex plasma surface. Beam quality is better.

These results suggest that if we are willing to settle for a well-behaved diverging beam we might get equally good or better results, with less beam loss on the extractor, by taking a "converging" Pierce geometry and running the beam in the opposite direction, from the smaller aperture toward the larger one.

Magnetic Field Shaping Experiment

Although the results of the constant perveance experiment suggest that the magnetic field in the extraction region is too weak to have a measurable affect on the accelerated ion trajectories, it does not follow that the field has no affect on the shape of the plasma boundary.

Figure 11 shows the location and geometry of an uncooled magnet, wound with #16 double daglas covered wire, which superimposes its necessarily weak aiding field on the distribution shown in Fig. 3.

The results obtained with this geometry can be summarized as follows:

A low perveance beam, none of which was intercepted by the magnet spool, stayed constant at approximately 38 mA while the magnet current in M-2 was varied from zero to 3.0 amperes. Beam radius decreased from 0.581 in. to 0.510 in. and beam divergence went from 0.110 to 0.095 rad.

For medium perveance source conditions, the beam current varied from 26 mA to 45 mA as the current in M-2 was varied from zero to 10 amperes (outgassing of the coils was quite severe at this current). Beam radius went from 0.619 in. to 0.594 in. and the divergence from 0.146 to a maximum of 0.149 and back down to 0.142 rad.

For high perveance source conditions, the beam current was constant at 32 mA while the beam radius went from 0.681 in. to 0.657 in. and the divergence went from 0.175 to 0.187 before dropping to 0.183 rad. M-2 current was varied from zero to 6 amperes.

In some of the medium and high perveance condition beam photographs there appears to be a very slight amount of barrel distortion.

A shorter coil with a somewhat larger bore which is not expected to intercept any of the beam has been wound but has not yet been installed and tested due to the press of other work.

The ideal field distribution would be one that expanded the plasma up to the proper size just ahead of the location of the ideal plane plasma boundary and then reversed its curvature to give a field that was parallel to the axis across the extraction gap. The forthcoming experiment with the shorter coil represents a rather crude first approximation to this ideal distribution, but one that may result in a useful reduction in beam divergence if it does not introduce serious aberrations.

Bench Test of Preaccelerator Extractor and Focus Electrode Geometry

Figure 12 shows a test bench mock-up of the extractor and focus electrode geometry chosen for initial tests of the column with the relatively high divergence beam from the present source. In the experiment shown, the extraction voltage, $\Delta V = V_3 - V_2$ was held

constant at 20 kV while the focus electrode voltage was varied from 12 to 32 kV. The data for Fig. 12 were taken after a trial run was made to obtain, roughly, beam power densities to be used in Eq. (9) for exposure time.

Source conditions for this experiment were adjusted to approximate the conditions at 20 kV in the constant perveance experiment of Fig. 8.

The results, self-explanatory, are shown in Figs. 12 and 13. For symmetrical beam images, we measure the diameter of the image on the photograph. In this case, however, with the right sides of the images distorted, we measured the radius to the left, on axis.

After this run was completed, the electrode assembly was examined and it was found that the spherical grid was dished in on one side. A correctly shaped grid will undoubtedly result in better beam quality.

Acknowledgements

The invaluable assistance of B. A. Richardson, D. S. Warren, and B. Perry (participants in the MURA-Antioch College of Ohio cooperative work-study program) in all phases of the experimental work is gratefully acknowledged.

References

1. J. Faure, Internal Report, SEFS TD 64/3, Source à Grande Brilliance.
2. J. A. Fasolo, Unpublished, 1965.
3. G. G. Kelley, N. H. Lazar, and O. B. Morgan, Nuc. Instr. & Meth. 10, 263-271 (1961).
4. J. A. Fasolo, Review of Hot-Cathode Ion Source Development for the Pulsed Magnetic Mirror Thermonuclear Reactor Program, UCRL 5285 (1958).
5. C. D. Curtis, Unpublished, 1966.
6. C. D. Curtis and J. A. Fasolo, Ion Beam Emittance Measurements with Source Point Correction, MURA TN-580 (unpublished).
7. K. R. Spangenberg, Vacuum Tubes, McGraw-Hill, New York (1940), p. 472.
8. H. Wroe, Some Measurements of the Emittance of the Output Beam of the AGS Duoplasmatron Ion Source, BNL HW-2 Internal Report (1966).
9. J. R. Pierce, Theory and Design of Electron Beams, 2d Ed. Chap. 2, D. Van Nostrand Company, Inc., Princeton, N. J. (1954).
10. M. Chodorow and C. Susskind, Fundamentals of Microwave Electronics, Chap. 2, McGraw-Hill, New York (1964).

DISCUSSION

J. A. FASOLO, MURA

SLUYTERS, BNL: In one of your last pictures you have shown emittances for the case in which your magnetic field penetrates quite far into your expansion cup. Nearly all the emittance pictures show brighter intensity on the outside than on the inside. Can this be caused by the magnetic fields inside the expansion cup?

FASOLO: We have aluminized the target from an external light and the black area you see is the reflection of the aluminized target of the window. In some of the other photographs, where the light isn't quite as strong, there is a darker area which, in some cases, seems to indicate that the

beam is brighter on the edges.

VOSICKI, CERN: May I comment on the ring-shaped beam you discussed with Dr. Sluyters? We made the same observations and found that the ring-shaped feature was due to screen fatigue. I had a hollow beam and wondered for quite a long time what it was. Then I focused the beam, and the dark spot became red; I focused it further, and the dark spot was still smaller and became yellow. It was the glowing of the screen. But also the aluminum coating can be spotted, and you can have less reflection on the spot where the beam usually falls. That can also be a reason for darkness in the center.

FASOLO: The coating doesn't last too long; we have to recoat it every week or so.

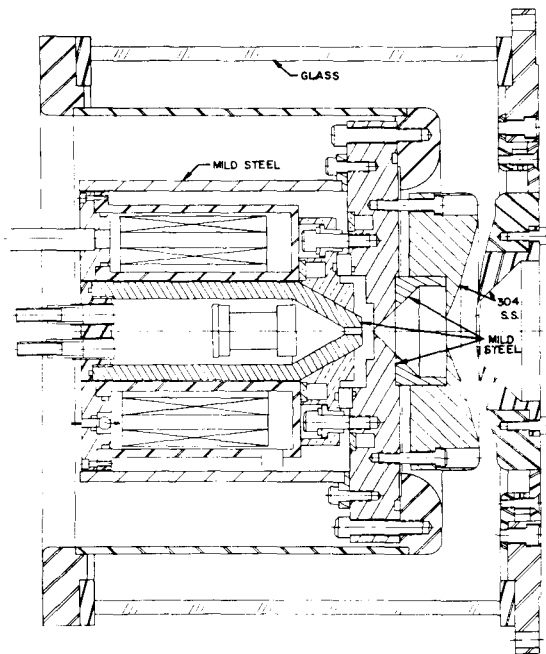


Fig. 1. Source assembly, Geometry 1.

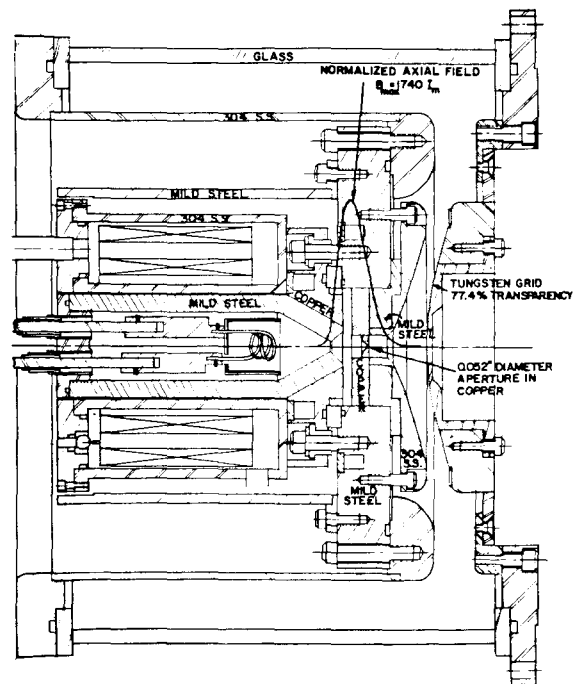


Fig. 2. Source assembly, Geometry 30.

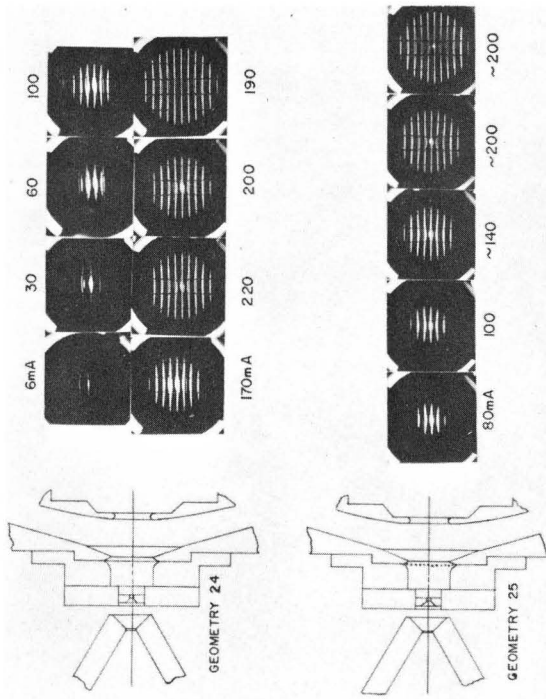


Fig. 4. Variation in beam current and quality as the magnetic field is increased for several extraction geometries.

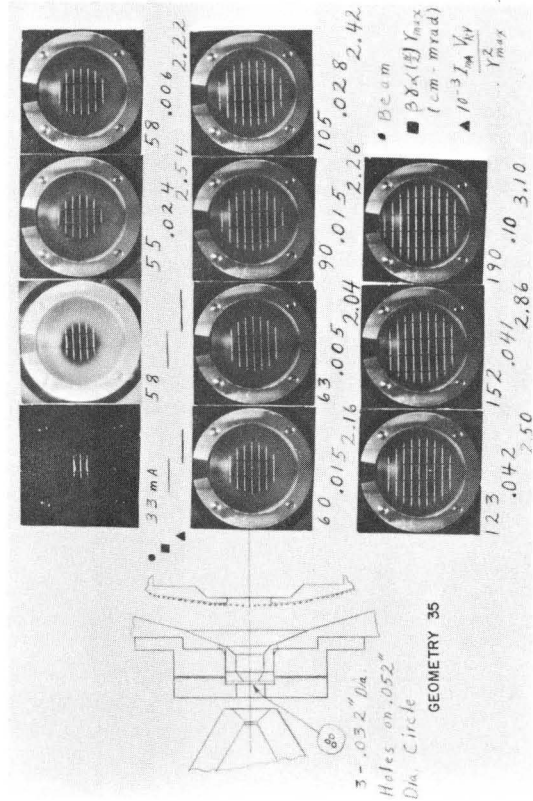


Fig. 6. Variation in beam current, beam emittance, and beam power density as the magnetic field is increased in Geometry 35.

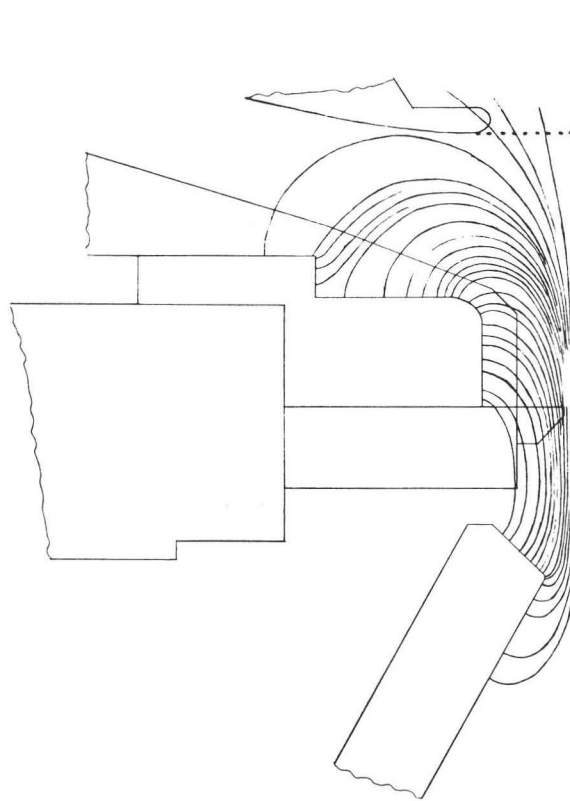


Fig. 3. Magnetic field distribution with Geometry 30 superimposed.

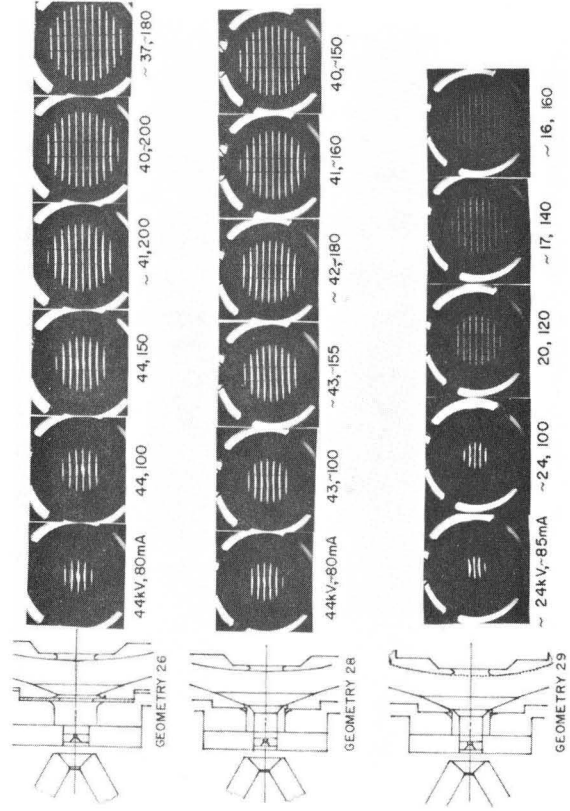


Fig. 5. Variation in beam current and quality as the magnetic field is increased for several extraction geometries.

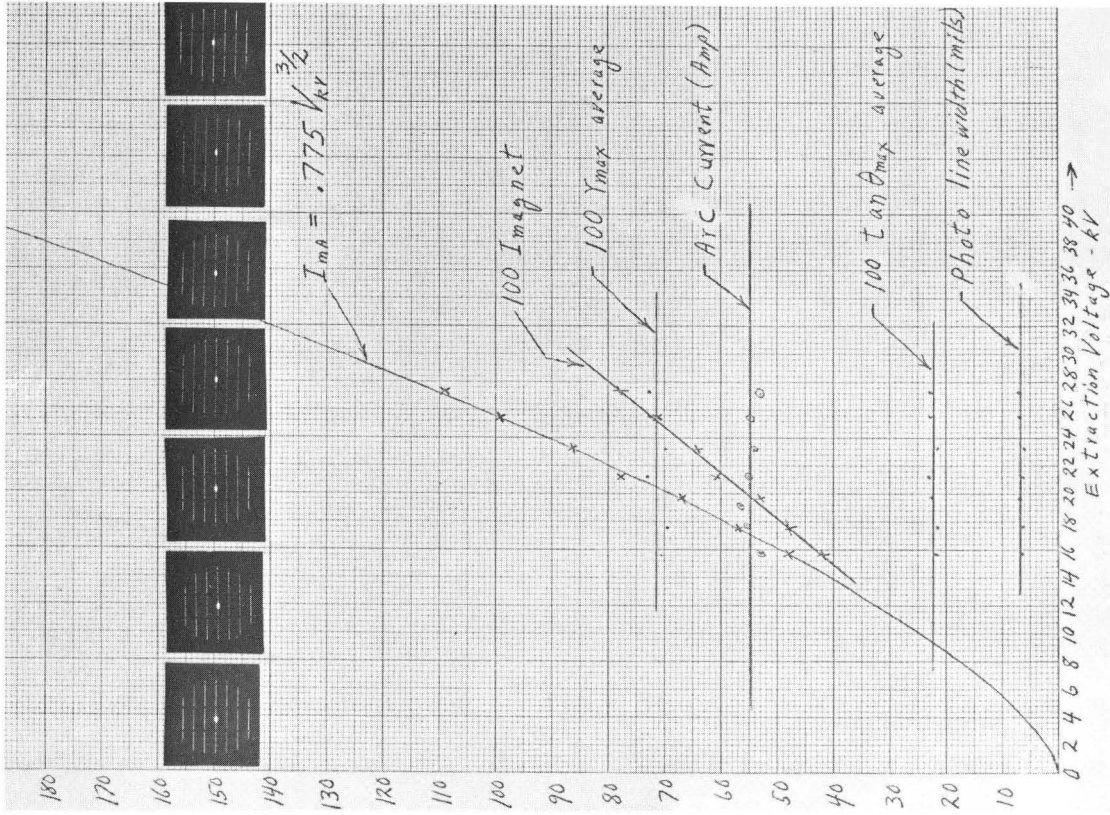


Fig. 8. Results of a constant perveance experiment.

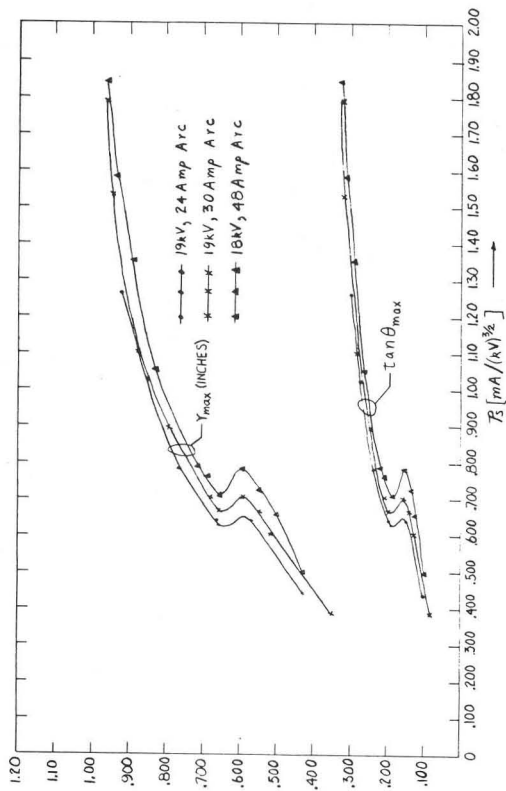


Fig. 7. Beam characteristic curves for Geometry 35.

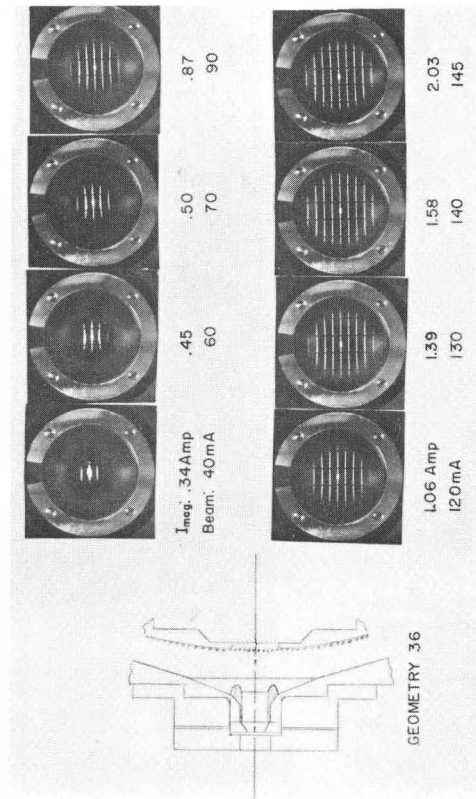


Fig. 9. Affect of beam quality of an imposed perturbation in the extraction geometry.

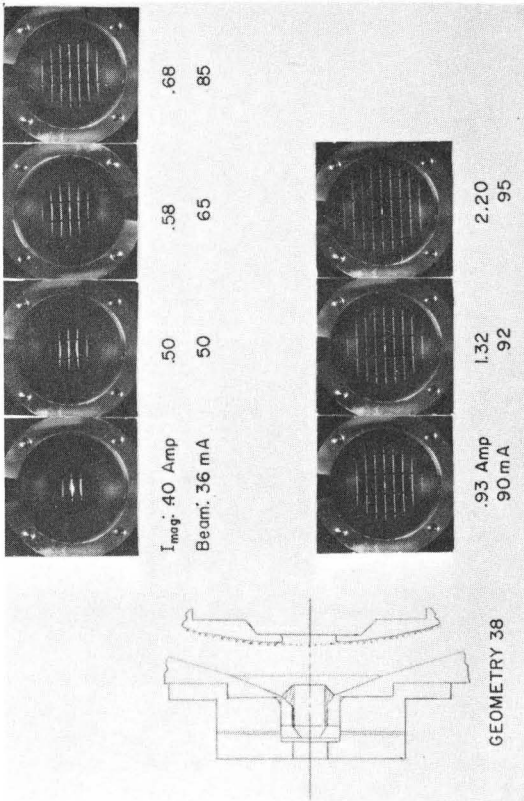


Fig. 10. Affect on beam quality of a modified perturbation in the extraction geometry.

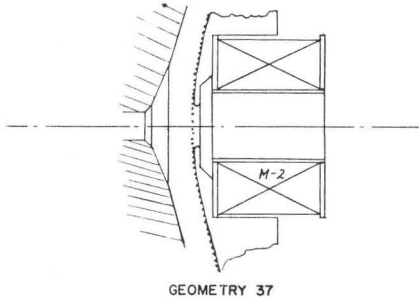


Fig. 11. Location and geometry of the extractor magnet.

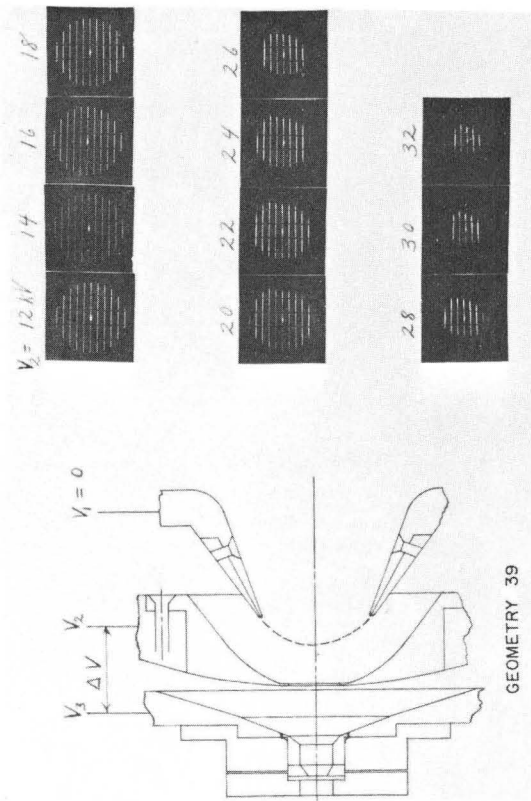


Fig. 12. Variation in beam quality with focus voltage, V_2 , as the extraction voltage, ΔV , is held constant at 20 kV in test bench mock-up of extractor and focus electrode geometry.

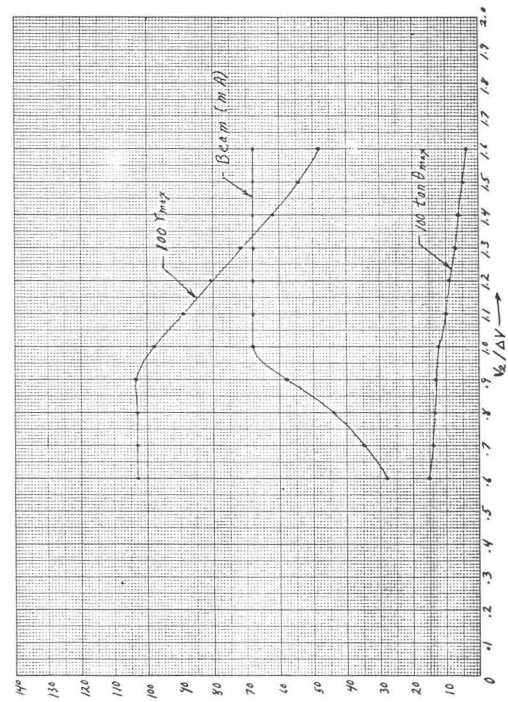


Fig. 13. Beam current, radius, and divergence vs $V_2/\Delta V$ for the data of Fig. 12.